CCS Chemistry

COMMUNICATION

Received: Dec. 16, 2024 | Accepted: Jan. 6, 2025 | Published: Feb. 15, 2025

Breaking the Boundary of Gigantic Molybdenum Blue Clusters: From Half-Closed {Mo_{85}} to {Mo_{172}} Dimer

Mengyuan Cheng[1†], Duidui Zhang[1†], Yingchao Liu[2†], Zeyu Chen[1], Yubin Ma[1], Rongqing Tang[1], Keying Wang[1], Heng Wang[2], De-Liang Long[3], Leroy Cronin[3]*, and Weimin Xuan[1]*

[1]*State Key Laboratory of Advanced Fiber Materials & College of Chemistry and Chemical Engineering, Donghua University, Shanghai 201620,* [2]*State Key Laboratory of Organometallic Chemistry, Shanghai Institute of Organic Chemistry, University of Chinese Academy of Sciences, Chinese Academy of Sciences, Shanghai 200032,* [3]*School of Chemistry, The University of Glasgow, Glasgow G12 8QQ*

**Corresponding authors: weiminxuan@dhu.edu.cn; lee.cronin@glasgow.ac.uk;* [†]M. Cheng, D. Zhang, and Y. Liu contributed equally to this work.

Cite this: *CCS Chem.* **2025**, Just Published. DOI: 10.31635/ccschem.025.202405353

Cyclic assemblies represent an important class of functional structures due to their inherent porous architectures and diverse properties. However, the controlled synthesis of cyclic aggregates with precise size, achieved by modulating the oligomerization of fundamental building blocks (BBs), remains a formidable challenge. Here we report the synthesis of the previously elusive octameric member of molybdenum blue (MB) wheels, {Mo_{85}} (1), and its dimer analogue {Mo_{172}} (2), under the direction of novel BBs of {Mo_1}, {Mo_2}, and bent {Mo_6} pentagon. The combination of these with existing BBs facilitates wheel contraction and distortion, resulting in the formation of an ellipitical and half-closed {Mo_{85}} octamer, the smallest cyclic cluster in the MB family. The {Mo_{172}} dimer exhibits cross-shaped architecture, composed of two {Mo_{86}} clusters structurally analogous to {Mo_{85}}. Moreover, the structural integrity of 1 and 2 was confirmed by mass spectrometry and other analytic techniques, enabling their exploration in photothermal conversion in both solution and the solid state.

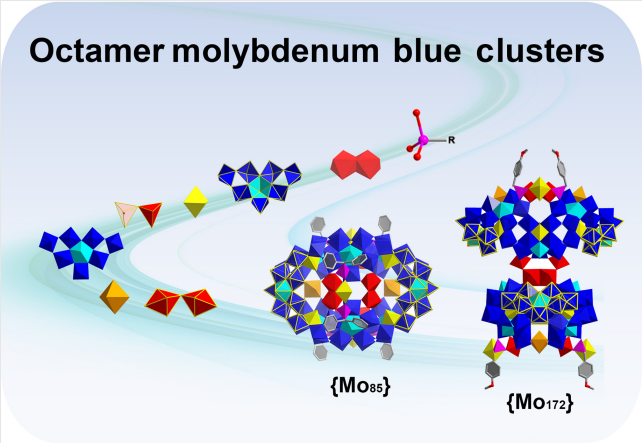

Keywords: **polyoxometalates, gigantic molybdenum blue cluster, octamer, building blocks, self-assembly**

Introduction

Polyoxometalates (POMs) are an intriguing class of inorganic clusters constructed from metal-oxygen building blocks (BBs), showing remarkable diversity in structures and properties.[1–13] Modulation of the way BBs self-assemble dictates not only the molecular structures of POMs but also their physicochemical properties, facilitating applications in catalysis, medicine, electronic devices, and magnetism.[14–23] Gigantic POMs, composed of hundreds of metal centers with size comparable to biomolecules, exemplify the cutting edge of controlled assembly. They showcase how rational combination of fundamental BBs can create complex and high-nuclearity clusters.[24–39]

Citation: *CCS Chem.* **2025**, Just Published. DOI: 10.31635/ccschem.025.202405353
Link to VoR: https://doi.org/10.31635/ccschem.025.202405353

Nevertheless, synthesizing gigantic POMs remains a significant challenge. The inherent difficulty lies in introducing new BBs and integrating them into the desired structures under controlled way.

Molybdenum blue (MB) is an archetypical class of gigantic wheel-shaped POM clusters that can be viewed as oligomeric assemblies of fundamental {Mo_8}, c-{Mo_2} (corner-shared {Mo_2}) and {Mo_1} BBs.[40–49] The central {Mo_6} pentagons within {Mo_8} BBs are crucial for the formation of wheel-shaped structures, while c-{Mo_2} BBs act as linkers between {Mo_6} BBs.[6] The well-defined BBs allow for the generation of a diverse MB family ranging from decameric enclosed {Mo_{132}} ({E-Mo_{132}}) to hexadecameric {Mo_{176}}, all built by varying the number of {Mo_8} BBs (Scheme 1).[41,42,50–54]

However, despite significant efforts, the synthesis of octamer remains elusive. Detailed analysis of representative MB clusters reveals a key factor: replacing c-{Mo_2} linkers with smaller e-{Mo_2} (edge-shared {Mo_2}) or lanthanide (Ln) ions induces the structural transformation from tetradecamer to dodecamer and decamer (Scheme 1).[41,42,50–54] Compared with c-{Mo_2}, these smaller linkers pull the adjacent {Mo_6} BBs closer together, resulting in increased strain.[52,55] To relieve this strain, the MB wheels tend to contract and adopt a lower oligomeric skeleton, as evidenced by the formation of dodecameric {$Mo_{120}Ce_6$}[52] and {$Mo_{124}Ce_4$}[53] and decameric {$Mo_{90}Ce_{10}$}[50] and {E-Mo_{132}}.[51] Considering this, it is reasonable to expect that introducing linkers even smaller than Ln ions might further induce wheel contraction and allow for the formation of an octamer.

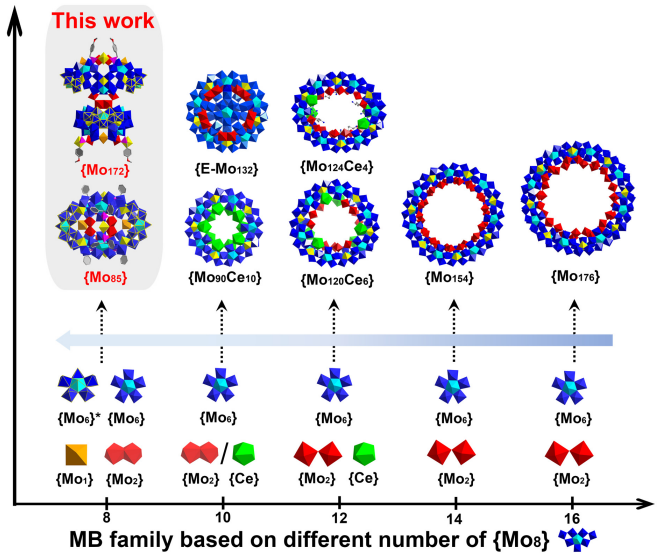

Scheme 1 | *Top: Schematic showing the structure evolution from hexadecameric {Mo_{176}} to octameric {Mo_{85}} and {Mo_{172}} (this work). Bottom: The linkers and pentagonal {Mo_6} BBs associated with the different oligomeric MB clusters.*

Recent study also indicates that classical convex pentagonal {Mo_6} in {Mo_8} can be replaced by concave {Mo_6} BB.[56] This leads to lantern type {Mo_{132}},[56] with the belt containing 10 sets of {Mo_8} arranged similarly to those in {$Mo_{90}Ce_{10}$} and {E-Mo_{132}}.[50,51] Moreover, a bent-type {Mo_6} BB has been observed in wheel-shaped {$Mo_{51}V_9$}[57] that consists of six sets of {Mo_8} BBs. This implies that variation of {Mo_6} BBs can also manipulate the degree of oligomerization. In this context, we propose that introducing new BBs with novel connection modes is a viable strategy for constructing MB octamer. These new BBs should also be compatible with the contraction and distortion required for the formation of smaller wheel-shaped structures.

Herein we report the synthesis of octameric missing link in MB family, {Mo_{85}} and its dimer analogue {Mo_{172}} (**1** and **2**). Both clusters are constructed by introducing novel {Mo_1}*, {Mo_1}$^{\#}$/{Mo_2}$^{\#}$ and bent pentagonal {Mo_6}* (within {Mo_8}*) along with e-{Mo_2} and {Mo_1} BBs (Figure 1). The combination of the smallest {Mo_1}* with e-{Mo_2} BBs effectively addresses the strain requirement for an octameric wheel, while the coupling of distorted {Mo_6}*/{Mo_8}* with {Mo_1}$^{\#}$/{Mo_2}$^{\#}$ facilitates the assembly of elliptical skeletons with reduced wheel strain; these

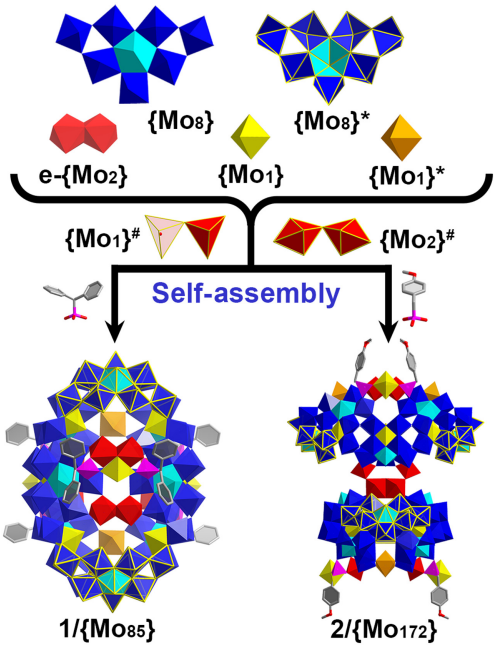

Figure 1 | *Assembly of **1** and **2** via combination of {Mo_1}*, {Mo_1}$^{\#}$/{Mo_2}$^{\#}$, and bent {Mo_6}* (within {Mo_8}*) with e-{Mo_2} and {Mo_1} BBs. {Mo_1}, yellow polyhedron, {Mo_1}*, orange polyhedron; {Mo_2}, red polyhedron; {Mo_1}$^{\#}$/{Mo_2}$^{\#}$, red polyhedron bordered in yellow wires, and one of the disorder position of {Mo_1}$^{\#}$ is highlighted in 50% transparency; {Mo_8}, blue polyhedron with central Mo in cyan; {Mo_8}*, same as {Mo_8} but bordered in yellow wires; C, grey; O, red; and P, purple.*

Citation: *CCS Chem.* **2025**, Just Published. DOI: 10.31635/ccschem.025.202405353
Link to VoR: https://doi.org/10.31635/ccschem.025.202405353

together enable the formation of {Mo_{85}} and {Mo_{172}}. {Mo_{85}} features an elliptical and half-closed wheel structure, whereas {Mo_{172}} adopts cross-shaped architecture dimerized from two {Mo_{86}} moieties (Figure 1). Given the intense absorption in the anear-infrared region, they are investigated for photothermal conversion under 808 nm laser irradiation. Both compounds are comprehensively characterized and formulated as follow (see Supporting Information Tables S1, S5 and Figures S1, S9–S17).

$Na(NH_4)_{10}H_9\{(Mo^{V}_{26}Mo^{VI}_{59}(OH)_{16}(H_2O)_{13}O_{238}(PO_3C_{13}H_{11})_6\} \cdot ca.95 \cdot H_2O \cdot \equiv \cdot Na(NH_4)_{10}H_9\{\mathbf{1a}\} \cdot ca.95 \cdot H_2O$ **1**/{**Mo_{85}**}

$K_{13}H_{11}\{Mo^{V}_{26}Mo^{VI}_{60}(OH)_{10}(H_2O)_{12}O_{242}(PO_3C_7H_6OCH_3)_4\}_2 \cdot ca.230 \cdot H_2O \cdot \equiv \cdot K_{13}H_{11}\{\mathbf{2a}\} \cdot ca.230 \cdot H_2O$ **2**/{**Mo_{172}**}

Results and Discussion

Hydrothermal reaction of molybdate under a highly reduction degree in the presence of organophosphonates afforded **1** and **2**. The high reducing ratio is crucial for the formation of e-{Mo_2^{V}} and {Mo_1^{V}}*, which are responsible for ring contraction. Similar to the role of acetate during the assembly of Keplerate {Mo_{132}} and {E-Mo_{132}},[51,58] organophosphonates might behave like structure-directing agents, triggering the formation of e-{Mo_2^{V}} through coordination. Moreover, the trigonal pyramidal distribution of three O atoms on organophosphonates enables more diverse binding modes and thus facilitates the growth of an additional {Mo_1} BB on the side of e-{Mo_2^{V}} via the μ_3-PO_3^{2-} coordination manner. If organophosphonates are absent from the synthesis, only unidentified precipitates are obtained.

Single-crystal X-ray structural analysis reveals that the octameric framework of **1a** is assembled from 6 {Mo_8}, 2 {Mo_8}*, 4 e-{Mo_2}, 9 {Mo_1}, and 2 {Mo_1}* BBs plus an interior {Mo_1}$^{\#}$ template which is disordered over two positions with each having half occupancy (Figure 1 and Supporting Information Figure S2). The 4 e-{Mo_2} BBs act as linkers to bridge six {Mo_8} BBs and can be classified into two types. The first type connects with two neighboring {Mo_8} BBs in a shoulder-to-shoulder mode on the open side of {Mo_{85}} (Figure 2a), while the other type links two {Mo_8} BBs in a head-to-head manner on the closed side (Figure 2b). As such, {Mo_{85}} adopts a half-closed architecture with the aperture sizes of ~9.0 × 3.3 Å (Supporting Information Figure S3). Half-closed gigantic POMs are quite rare, with only {Mo_{180}}[59] and {$Ce_{11}Mo_{96}$}[51] reported so far. Moreover, an extra {Mo_1} BB is attached to e-{Mo_2} with aid of two diphenyl methylphosphonate ligands (Figure 2a). On the other hand, two {Mo_1}* BBs can also connect with two {Mo_8} BBs in a shoulder-to-shoulder manner (Figure 2a), reminiscent of the {Mo_1} in ball-like {Mo_{102}}.[60] Notably, bond valence sum calculations further confirm {Mo_1}* also adopts as +5 oxidation state (Supporting Information Tables S2–S4).[61] In contrast to the {Mo_1^{VI}} BBs located below pentagonal {Mo_6} or attached on the surface of **1a**, {Mo_1}* BB behaves as an essential linker that is responsible for the ring distortion and contraction. Overall, the self-assembly involving 6 {Mo_8} guided by 4 e-{Mo_2} and 2 {Mo_1}* linkers yields the core structure of {Mo_{85}}, which is functionalized by six organophosphonate on the surface and exhibits an elliptical architecture (Figure 2a, dotted box).

The {Mo_6}* unit in {Mo_8}* adopts bent configuration, with one vertex Mo atom significantly deviated from the plane defined by other five Mo atoms (Figure 2c and Supporting Information Figure S4). The unique configuration of {Mo_6}* is similar to that in {$Mo_{51}V_9$},[57] providing a novel pentagonal BB complementary to convex[41] and concave {Mo_6}.[58] As a result, {Mo_8}* assumes a hook-like arrangement, allowing it to bind to the core structure in a more bent orientation (Figure 2d and Supporting Information Figure S5). Consequently, two {Mo_8}* BBs form the most elliptical parts at the two ends of {Mo_{85}}

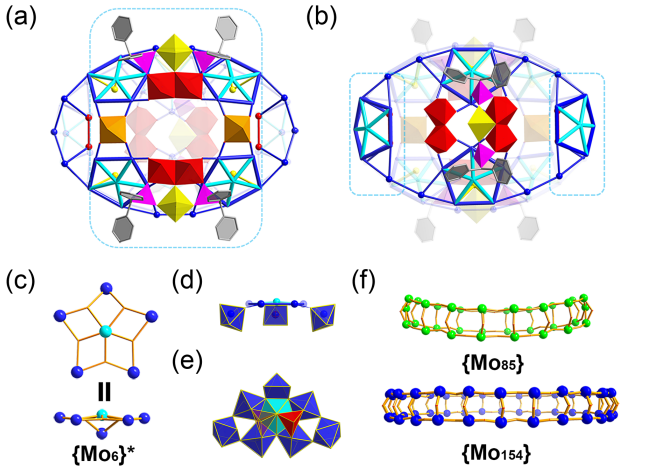

Figure 2 | *View of the simplified framework of **1a** showing both (a) the open and (b) the closed sides. The core structure and hook-like {Mo_8}* are highlighted in dotted boxes, respectively. (c) View of bent {Mo_6}*, (d) hook-like {Mo_8}*, and (e) square pyramidal {Mo_1}$^{\#}$ template below {Mo_8}*. (f) Different arrangement of equators for **1a** and {Mo_{154}}. Color scheme is the same as Figure 1.*

Citation: *CCS Chem.* **2025**, Just Published. DOI: 10.31635/ccschem.025.202405353
Link to VoR: https://doi.org/10.31635/ccschem.025.202405353

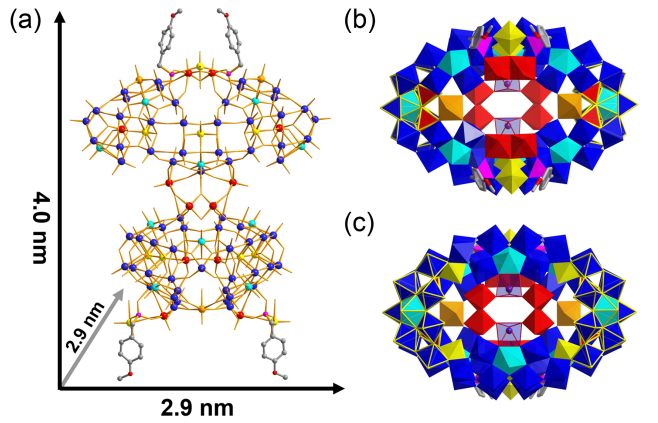

Figure 3 | *(a) Side view of {Mo$_{172}$}. (b, c) Top view of the {Mo$_{86}$} monomer in {Mo$_{172}$} from two sides. The square pyramidal Mo atoms in {Mo$_6$} BBs are highlighted in transparent polyhedron.*

(Figure 2b, dotted box). Additionally, a {Mo$_1$}$^{\#}$ template is situated at the back of the {Mo$_8$}* and disordered over two positions with half occupancy (Figure 2e). To differentiate from well-established {Mo$_2$} BBs in MB clusters, one of the disordered Mo positions in {Mo$_1$}$^{\#}$ is highlighted in transparence (Figure 1). While {Mo$_{85}$} exhibits the largest aspect ratio (1.50) among all reported MB,[62] its equator adopts a tensioned boat-like configuration to further alleviate the strain, unlike the almost coplanar arrangement observed in other MB clusters like {Mo$_{154}$}[41] (Figure 2f and Supporting Information Figure S6). On the whole, the successful construction of **1** validates our hypothesis that introducing smaller linkers and new BBs compatible with wheel contraction and distortion is a promising approach for achieving octameric MB cluster.

2a features a dimeric structure built from two {Mo$_{86}$} clusters linked via two sets of e-{Mo$_2$} on separate wheels (Figure 3a). Owing to the twisting of one {Mo$_{86}$} relative to the other around the C_4 axis by an angle of 90°, **2a** adopts cross-shaped architecture with approximate dimensions of 4.0 × 2.9 × 2.9 nm (Figure 3a). {Mo$_{86}$} also possesses an octameric skeleton but is composed of six{Mo$_8$}, two {Mo$_8$}*, four e-{Mo$_2$}, two{Mo$_2$}$^{\#}$, eight {Mo$_1$}, and two {Mo$_1$}* BBs (Figure 3b). Therefore, {Mo$_{86}$} can be viewed as a structural analogue of {Mo$_{85}$} with some key differences: (1) In contrast to traditional octahedral configuration, the vertex Mo atoms in two {Mo$_6$} BBs adopt square pyramidal coordination environment (Figure 3b,c). Also, {Mo$_1$} BB is eliminated from the side of e-{Mo$_2$} to minimize the steric hindrance between two {Mo$_{86}$}; (2) The Mo atoms in {Mo$_2$}$^{\#}$ units exhibit triangular bipyramid configuration rather than square pyramidal {Mo$_1$}$^{\#}$ in {Mo$_{85}$} (Supporting Information Figure S7). The spontaneous generation of dimeric {Mo$_{172}$} clearly manifests that the gigantic MB clusters are available in the solution for high-order assembly into even more complex and diverse aggregates; this has already led to the discovery of dimeric {Mo$_{256}$Eu$_8$}, {Mo$_{200}$Ce$_{12}$}, and {Mo$_{240}$Ce$_{12}$}.[62–64]

Electrospray ionization-traveling wave ion mobility mass spectrometry (ESI-TWIM-MS) is useful for investigating the structures in solution, and spectra were acquired for compounds **1** and **2**. As shown in Figure 4a, the molecular species for compound **1** could be detected at

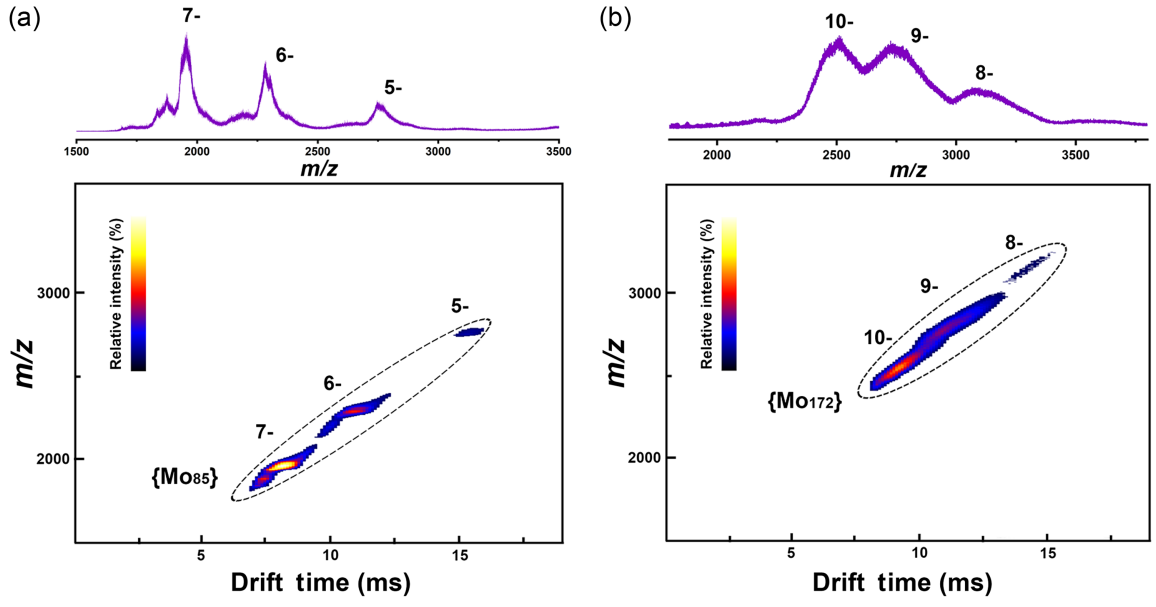

Figure 4 | *ESI-TWIM-MS plots (m/z vs drift time) of aqueous solution of **1** and **2**. Relative intensity (cf. highest peak) is shown on a linear scale (using the colored scale, inset).*

Citation: *CCS Chem.* **2025**, Just Published. DOI: 10.31635/ccschem.025.202405353
Link to VoR: https://doi.org/10.31635/ccschem.025.202405353

Table 1 | *Assignment of Peaks of **1** and **2***

Identification of **1**	*Z*	m/z_{cal}	m/z_{obs}	Identification of **2**	*Z*	m/z_{cal}	m/z_{obs}
$\{Mo_{85}O_{238}(PO_3C_{13}H_{11})_6(OH)_{16}H_{13}\}$	−7	1960.7	1960.0	$\{Mo_{172}O_{484}(PO_3C_7H_6OCH_3)_8(OH)_{20}H_{14}\}$	−10	2620.6	2620.0
$\{Mo_{85}O_{238}(PO_3C_{13}H_{11})_6(OH)_{16}H_{14}\}$	−6	2287.6	2287.5	$\{Mo_{172}O_{484}(PO_3C_7H_6OCH_3)_8(OH)_{20}H_{15}\}$	−9	2911.2	2912.5
$\{Mo_{85}O_{238}(PO_3C_{13}H_{11})_6(OH)_{16}H_{15}\}$	−5	2745.4	2745.7	$\{Mo_{172}O_{484}(PO_3C_7H_6OCH_3)_8(OH)_{20}H_{16}\}$	−8	3275.3	3275.3

negative charges from −5 to −7 by losing different numbers of cations. Despite the broad peak envelopes observed in the spectra, it is a common phenomenon in ESI-MS of giant POMs, caused by the association of counterions and solvent molecules.[65,66] The major peaks in the spectrum of 1 can be assigned to the formula $[Mo_{85}O_{238}(PO_3C_{13}H_{11})_6(OH)_{16}]$ (Table 1). Similarly, all the major peaks of compound **2** in the spectrum can be assigned to the formula $[Mo_{172}O_{484}(PO_3C_7H_6OCH_3)_8(OH)_{20}]$, with charges from −8 to −10 (Figure 4b and Table 1). This represents weak evidence of intact rings. However, the 2D ion mobility data separated by the TWIM (Figure 4) demonstrates that one main rigid size/shape dominates. The stability of **1** and **2** was further confirmed by UV–vis-NIR and Fourier transform infrared (FT-IR) study of their tetrabutylammonium (TBA) salts, **TBA-1** and **TBA-2** (Supporting Information Figure S12), as evidenced by similar profiles of **TBA-1** and **TBA-2** to **1** and **2** as well as negligible degradation for 24 h in related spectra (Supporting Information Figures S13–S16).

MB clusters are well known for their intense absorption spanning from visible to near-infrared regions due to the intervalence $Mo^{V}\rightarrow Mo^{VI}$ charge transfer.[67,68] This unique property renders them ideal candidates for photothermal conversion.[69–71] Hence, we investigated the photothermal performance of **1** and **2** by measuring their temperature response with various concentrations under 808 nm laser irradiation (Supporting Information Figures S18–S21). Control experiments using blank CH_3CN solution showed negligible temperature rise (<1 °C) (Figure 5a and Supporting information Figures S18–S19). In contrast, the plateau temperatures reached the optimal values of 75.6 °C and 77 °C for **1** and **2**,

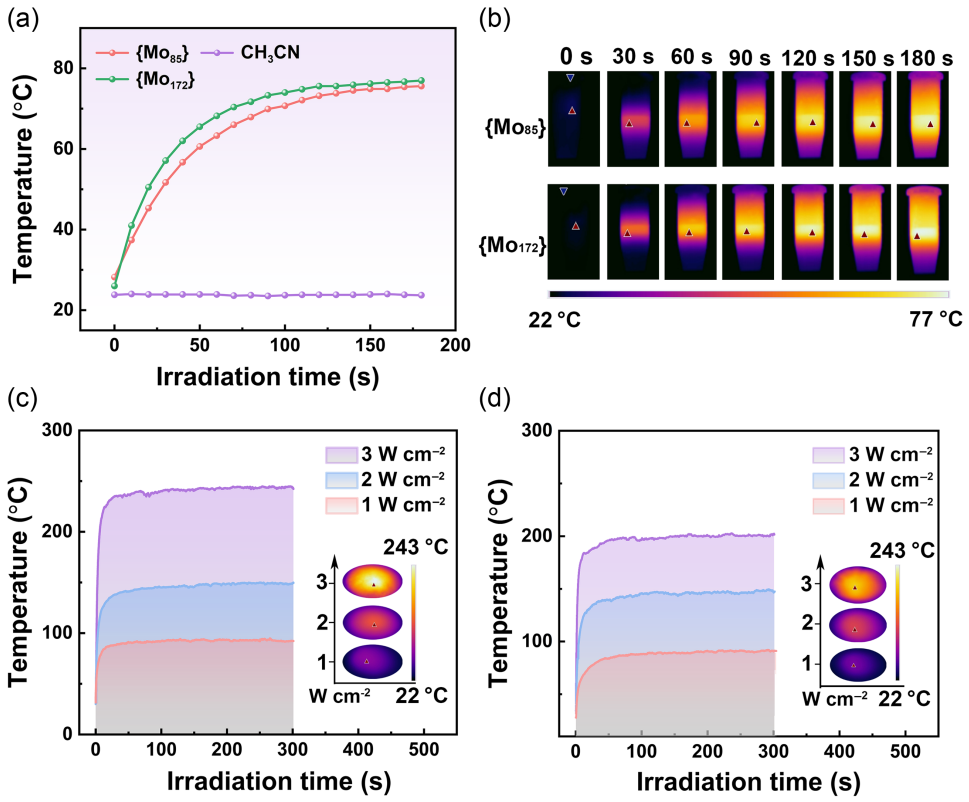

Figure 5 | *(a) Photothermal conversion curves of **1** (25 μM), **2** (25 μM), and blank CH_3CN under 808 nm laser irradiation (2 W cm^{-2}). (b) NIR thermal images of **1** and **2** (25 μM, 808 nm, 2 W cm^{-2}). Photothermal conversion curves of **1** (c) and **2** (d) in the solid state under 808 nm laser irradiation (1, 2, and 3 W cm^{-2}). Insets: the thermal images of **1** and **2** at highest temperature with different laser power densities.*

Citation: *CCS Chem.* **2025**, Just Published. DOI: 10.31635/ccschem.025.202405353
Link to VoR: https://doi.org/10.31635/ccschem.025.202405353

respectively (Figure 5a,b). Notably, the maximum temperatures remained almost unchanged for six heating and cooling cycles, demonstrating the excellent photothermal stabilities of both clusters (Supporting Information Figure S20). Calculations revealed a photothermal conversion efficiency of 50.1% for **1** and 41.3% for **2** (Supporting Information Figures S22 and S23). As depicted in Figure 5c,d, the plateau temperature of **1** reached 86.3 °C in 15.8 s (1 W cm^{-2}), a much higher heating rate compared to **2** (82.9 °C in 40.5 s). A similar trend was observed at 3 W cm^{-2}, and the maximum temperature of 243 °C was obtained for **1** within a shorter radiation time (Figure 5c,d). This probably arises from the stronger absorption at 808 nm for **1** than that of **2** (Supporting Information Figure S24).

Conclusion

In summary, we have successfully synthesized two unprecedented wheel-shaped clusters, $\{Mo_{85}\}$ and $\{Mo_{172}\}$, which feature octameric architectures and fill a critical gap in the gigantic MB family. The controlled assembly of these cyclic structures was achieved through novel connection modes enabled by $\{Mo_1\}^*$, $\{Mo_1\}^{\#}/\{Mo_2\}^{\#}$, and pentagonal $\{Mo_6\}^*$ BBs, facilitating the necessary wheel contraction and distortion to form the smallest octamer. ESI-TWIM-MS study of **1** and **2**, along with UV–vis-NIR and FT-IR analysis of TBA-**1** and TBA-**2**, validated the stability and availability of $\{Mo_{85}\}$ and $\{Mo_{172}\}$ in solution. Furthermore, both compounds displayed photothermal effect in solution and the solid state. This work not only expands the structural diversity of gigantic MB clusters, but also paves the way to synthesize high-nuclearity clusters by introducing novel BBs with new connection modes.

Supporting Information

Supporting Information is available and includes detailed experimental procedures, characterizations, additional Figures S1–S24 and Tables S1–S5. Crystallographic data for the structures in this article has been deposited at the Cambridge Crystallographic Data Centre under deposition nos. CCDC 2373786-2373787.

Conflict of Interest

There is no conflict of interest to report.

Funding Information

This work was supported by the National Natural Science Foundation of China (grant nos. 92161111, 52372040, and 21901038), the Program for Professor of Special Appointment (Eastern Scholar) at the Shanghai Institutions of Higher Learning, the International Cooperation Fund of Science and Technology Commission of Shanghai Municipality (grant no. 21130750100), and the Strategic Priority Research Program of the Chinese Academy of Sciences (grant no. XDB0610000). We thank the staff from the College of Materials Science and Engineering (Donghua University) for X-ray data collection using Bruker D8 Venture and the staff from the BL17B1 beamline of the National Facility for Protein Science in Shanghai at the Shanghai Synchrotron Radiation Facility, for assistance during data collection. We also gratefully acknowledge financial support from the Engineering and Physical Sciences Research Council (EPSRC) (grant nos. EP/L023652/1, EP/R009902/1, EP/R020914/1, EP/R01308X/1, EP/S017046/1, EP/S019472/1, and EP/V048341/1), the European Research Council (Project 670467 SMART-POM), and the University of Glasgow.

References

1. Pope, M. T.; Müller, A. *Polyoxometalate Chemistry from Topology via Self-Assembly to Applications*; Kluwer Academic Publishers: Dordrecht, **2002**.
2. Long, D.-L.; Burkholder, E.; Cronin, L. Polyoxometalate Clusters, Nanostructures and Materials: From Self Assembly to Designer Materials and Devices. *Chem. Soc. Rev.* **2007**, *36*, 105–121.
3. Du, D.-Y.; Yan, L.-K.; Su, Z.-M.; Li, S.-L.; Lan, Y.-Q.; Wang, E.-B. Chiral Polyoxometalate-Based Materials: From Design Syntheses to Functional Applications. *Coord. Chem. Rev.* **2013**, *257*, 702–717.
4. Dolbecq, A.; Dumas, E.; Mayer, C. R.; Mialane, P. Hybrid Organic–Inorganic Polyoxometalate Compounds: From Structural Diversity to Applications. *Chem. Rev.* **2010**, *110*, 6009–6048.
5. Cadot, E.; Sokolov, M. N.; Fedin, V. P.; Simonnet-Jégat, C.; Floquet, S.; Sécheresse, F. A Building Block Strategy to Access Sulfur-Functionalized Polyoxometalate Based Systems Using $\{Mo_2S_2O_2\}$ and $\{Mo_3S_4\}$ as Constitutional Units, Linkers or Templates. *Chem. Soc. Rev.* **2012**, *41*, 7335–7353.
6. Müller, A.; Gouzerh, P. From Linking of Metal-Oxide Building Blocks in a Dynamic Library to Giant Clusters with Unique Properties and Towards Adaptive Chemistry. *Chem. Soc. Rev.* **2012**, *41*, 7431–7463.
7. Rausch, B.; Symes, M. D.; Chisholm, G.; Cronin, L. Decoupled Catalytic Hydrogen Evolution from a Molecular Metal Oxide Redox Mediator in Water Splitting. *Science* **2014**, *345*, 1326–1330.
8. Zhang, H.; Li, A.; Li, K.; Wang, Z.; Xu, X.; Wang, Y.; Sheridan, M. V.; Hu, H.-S.; Xu, C.; Alekseev, E. V.; Zhang, Z.; Yan, P.; Cao, K.; Chai, Z.; Albrecht-Schönzart, T. E.; Wang, S. Ultrafiltration Separation of Am(VI)-Polyoxometalate from Lanthanides. *Nature* **2023**, *616*, 482–487.
9. Li, Z.; Lv, Z.-H.; Yu, H.; Sun, Y.-Q.; Li, X.-X.; Zheng, S.-T. Giant Ln_{30}-Cluster-Embedded Polyoxotungstate Nanoclusters with Exceptional Proton-Conducting and Luminescent Properties. *CCS Chem.* **2022**, *4*, 2938–2945.

Citation: *CCS Chem.* **2025**, Just Published. DOI: 10.31635/ccschem.025.202405353
Link to VoR: https://doi.org/10.31635/ccschem.025.202405353

10. Chen, Y.; Guo, Z.-W.; Li, X.-X.; Zheng, S.-T.; Yang, G.-Y. Multicomponent Cooperative Assembly of Nanoscale Boron-Rich Polyoxotungstates with 22 and 30 Boron Atoms. *CCS Chem.* **2022**, *4*, 1305–1314.
11. Dai, Y.-C.; Zhang, S.-Y.; Xiao, X.-X.; Li, M.-J.; Liu, J.-C.; Chen, L.-J.; Zhao, J.-W. A Double-Tartrate-Bridged Deca-Nuclearity Europium-Tungsten Cluster Embedded Seleno-tungstate and Its Selective Optical Sensing of o-Nitrophenol. *Polyoxometalates* **2023**, *2*, 9140041.
12. Zhang, S.-W.; Huang, G.-Q.; Shao, M.-C.; Tang, Y.-Q. Crystal Structure of a Novel Mixed Valence Mo^{V}–Mo^{VI} Heteropolymolybdate Cluster: $[H_3O^+]_6[Mo_{57}V_6O_{183}(NO)_6(H_2O)_{18}]^{6-} \cdot 89H_2O$. *Chem. Commun.* **1993**, *1*, 37–38.
13. Zhang, S.-W.; Wei, Y.-G.; Yu, Q.; Shao, M.-C.; Tang, Y.-Q. Toward Quantum Line-Self-Assembly Process of Nanomolecular Building Blocks Leading to a Novel One-Dimensional Nanomolecular Polymer: Single-Crystal X-Ray Structure of $\{[H_3O]^+_{12}\{(H_2O)MoO_{2.5}[Mo_{36}O_{108}(NO)_4(H_2O)_{16}]O_{2.5}Mo(H_2O)\}^{12-}\}_n$. *J. Am. Chem. Soc.* **1997**, *119*, 6440–6441.
14. Ma, X.-Q.; Xiao, H.-P.; Chen, Y.; Lai, Q.-S.; Li, X.-X.; Zheng, S.-T. Polyoxometalate-Based Macrocycles and Their Assembly. *Coord. Chem. Rev.* **2024**, *510*, 215818.
15. Yonesato, K.; Yanai, D.; Yamazoe, S.; Yokogawa, D.; Kikuchi, T.; Yamaguchi, K.; Suzuki, K. Surface-Exposed Silver Nanoclusters Inside Molecular Metal Oxide Cavities. *Nat. Chem.* **2023**, *15*, 940–947.
16. Lu, M.; Zhang, M.; Liu, J.; Yu, T.-Y.; Chang, J.-N.; Shang, L.-J.; Li, S.-L.; Lan, Y.-Q. Confining and Highly Dispersing Single Polyoxometalate Clusters in Covalent Organic Frameworks by Covalent Linkages for CO_2 Photoreduction. *J. Am. Chem. Soc.* **2022**, *144*, 1861–1871.
17. Long, D.-L.; Tsunashima, R.; Cronin, L. Polyoxometalates: Building Blocks for Functional Nanoscale Systems. *Angew. Chem. Int. Ed.* **2010**, *49*, 1736–1758.
18. AlDamen, M. A.; Clemente-Juan, J. M.; Coronado, E.; Martí-Gastaldo, C.; Gaita-Ariño, A. Mononuclear Lanthanide Single-Molecule Magnets Based on Polyoxometalates. *J. Am. Chem. Soc.* **2008**, *130*, 8874–8875.
19. Xia, Y.-S.; Zhang, L.; Lu, J.-N.; Zhao, X.-H.; Dong, L.-Z.; Liu, J.; Lan, Y.-Q. A Triple Tandem Reaction for the Upcycling of Products from Poorly Selective CO_2 Photoreduction Systems. *Nat. Synth.* **2024**, *3*, 406–418.
20. Wang, S.-S.; Yang, G.-Y. Recent Advances in Polyoxometalate-Catalyzed Reactions. *Chem. Rev.* **2015**, *115*, 4893–4962.
21. Song, N.; Lu, M.; Liu, J.; Lin, M.; Shangguan, P.; Wang, J.; Shi, B.; Zhao, J. A Giant Heterometallic Polyoxometalate Nanocluster for Enhanced Brain-Targeted Glioma Therapy. *Angew. Chem. Int. Ed.* **2024**, *63*, e202319700.
22. Shang, Q.; Shen, K.; Zhao, D.; Wang, X.; Wei, Y.; Wang, H.; Wang, G.; Zhang, D.; Niu, J. Rare-Earth-Induced Peroxo-Phosphotungstates: Enhanced Proton Conductivity in Corresponding Membranes. *Polyoxometalates* **2025**, *4*, 9140077.
23. Li, H.-L.; Zhang, M.; Lian, C.; Lang, Z.-L.; Lv, H.; Yang, G.-Y. Ring-Shaped Polyoxometalate Built by $\{Mn_4PW_9\}$ and PO_4 Units for Efficient Visible-Light-Driven Hydrogen Evolution. *CCS Chem.* **2021**, *3*, 2095–2103.
24. Chen, H.; Zhang, M.; Li, Y.; Ma, P.; Wang, J.; Niu, J. Hexameric Polyoxotantalate with Proton Conduction Properties. *Chem. Commun.* **2023**, *59*, 10664–10667.
25. Liu, J.-C.; Zhao, J.-W.; Streb, C.; Song, Y.-F. Recent Advances on High-Nuclear Polyoxometalate Clusters. *Coord. Chem. Rev.* **2022**, *471*, 214734.
26. Kastner, K.; Puscher, B.; Streb, C. Self-Assembly of a Tetrahedral 58-Nuclear Barium Vanadium Oxide Cluster. *Chem. Commun.* **2013**, *49*, 140–142.
27. Sheng, H.-X.; Lin, B.-Y.; Chen, C.-Q.; Du, J.; Yang, P. From Confined Growth to Enhanced Peroxidase-Like Activity: Nucleation of a Phosphate-Mediated Fe^{III}–Ce^{III}–Oxo Cluster inside the $\{P_8W_{48}\}$ Nanoreactor. *Polyoxometalates* **2024**, *3*, 9140060.
28. Liu, W.-D.; Zhu, H.-T.; Zhang, X.; Su, F.; Sang, X.-J.; Zhang, X.-L.; Zhang, L.-C. Room Temperature Self-Assembly and Nonenzymatic Electrochemical Sensing Performance of Transition Metal-Embedded Wheel-Shaped Tungstophosphates. *Polyoxometalates* **2025**, *4*, 9140073.
29. Bassil, B. S.; Dickman, M. H.; Römer, I.; vonderKammer, B.; Kortz, U. The Tungstogermanate $[Ce_{20}Ge_{10}W_{100}O_{376}(OH)_4(H_2O)_{30}]^{56-}$: A Polyoxometalate Containing 20 Cerium(III) Atoms. *Angew. Chem. Int. Ed.* **2007**, *46*, 6192–6195.
30. Bannani, F.; Floquet, S.; Leclerc-Laronze, N.; Haouas, M.; Taulelle, F.; Marrot, J.; Kögerler, P.; Cadot, E. Cubic Box Versus Spheroidal Capsule Built from Defect and Intact Pentagonal Units. *J. Am. Chem. Soc.* **2012**, *134*, 19342–19345.
31. Wu, Y.; Li, X.; Qi, Y.; Yu, H.; Jin, L.; Zheng, S.-T. $\{Nb_{288}O_{768}(OH)_{48}(CO_3)_{12}\}$: A Macromolecular Polyoxometalate with Close to 300 Niobium Atoms. *Angew. Chem. Int. Ed.* **2018**, *57*, 8572–8576.
32. Zhu, M.; Han, S.; Liu, J.; Tan, M.; Wang, W.; Suzuki, K.; Yin, P.; Xia, D.; Fang, X. $\{Mo_{126}W_{30}\}$: Polyoxometalate Cages Shaped by π–π Interactions. *Angew. Chem. Int. Ed.* **2022**, *61*, e202213910.
33. DelaOliva, A. R.; Sans, V.; Miras, H. N.; Yan, J.; Zang, H.; Richmond, C. J.; Long, D.; Cronin, L. Assembly of a Gigantic Polyoxometalate Cluster $\{W_{200}Co_8O_{660}\}$ in a Networked Reactor System. *Angew. Chem. Int. Ed.* **2012**, *51*, 12759–12762.
34. Guan, Y.; Xiao, H.-P.; Li, X.-X.; Zheng, S.-T. Recent Advances on the Synthesis, Structure, and Properties of Polyoxotantalates. *Polyoxometalates* **2023**, *2*, 9140023.
35. Huang, G.-Q.; Zhang, S.-W.; Shao, M.-C. The Remarkable Polymetallate Cluster: Crystal Structure of $Na_6[H_6Mo_{57}Fe_6O_{183}(NO)_6(H_2O)_{18}] \cdot 91H_2O$. *Polyhedron* **1993**, *12*, 2067–2068.
36. Long, D.-L.; Cronin, L. Chapter Seven-Advances in Gigantic Polyoxomolybdate Chemistry. In *Recent Highlights I*; Hubbard, C. D., Eldik, R. van, Eds.; Advances in Inorganic Chemistry; Academic Press, **2021**; Vol. 78, pp 227–267.
37. Sommers, J. A.; Palys, L.; Martin, N. P.; Fast, D. B.; Amiri, M.; Nyman, M. Oxo-Cluster-Based Zr/Hf ^{IV} Separation: Shedding Light on a 70-Year-Old Process. *J. Am. Chem. Soc.* **2022**, *144*, 2816–2824.

Citation: *CCS Chem.* **2025**, Just Published. DOI: 10.31635/ccschem.025.202405353
Link to VoR: https://doi.org/10.31635/ccschem.025.202405353

38. Colliard, I.; Brown, J. C.; Fast, D. B.; Sockwell, A. K.; Hixon, A. E.; Nyman, M. Snapshots of Ce_{70} Toroid Assembly from Solids and Solution. *J. Am. Chem. Soc.* **2021**, *143*, 9612–9621.
39. Lin, J.; Li, N.; Yang, S.; Jia, M.; Liu, J.; Li, X.-M.; An, L.; Tian, Q.; Dong, L.-Z.; Lan, Y.-Q. Self-Assembly of Giant Mo_{240} Hollow Opening Dodecahedra. *J. Am. Chem. Soc.* **2020**, *142*, 13982–13988.
40. Müller, A.; Meyer, J.; Krickemeyer, E.; Diemann, E. Molybdenum Blue: A 200 Year Old Mystery Unveiled. *Angew. Chem. Int. Ed. Engl.* **1996**, *35*, 1206–1208.
41. Müller, A.; Krickemeyer, E.; Meyer, J.; Bögge, H.; Peters, F.; Plass, W.; Diemann, E.; Dillinger, S.; Nonnenbruch, F.; Randerath, M.; Menke, C. $[Mo_{154}(NO)_{14}O_{420}(OH)_{28}(H_2O)_{70}]^{(25\pm5)-}$: A Water-Soluble Big Wheel with More than 700 Atoms and a Relative Molecular Mass of About 24000. *Angew. Chem. Int. Ed. Engl.* **1995**, *34*, 2122–2124.
42. Müller, A.; Krickemeyer, E.; Bögge, H.; Schmidtmann, M.; Beugholt, C.; Kögerler, P.; Lu, C. Formation of a Ring-Shaped Reduced "Metal Oxide" with the Simple Composition $[(MoO_3)_{176}(H_2O)_{80}H_{32}]$. *Angew. Chem. Int. Ed.* **1998**, *37*, 1220–1223.
43. Miras, H. N.; Cooper, G. J. T.; Long, D.-L.; Bögge, H.; Müller, A.; Streb, C.; Cronin, L. Unveiling the Transient Template in the Self-Assembly of a Molecular Oxide Nanowheel. *Science* **2010**, *327*, 72–74.
44. Müller, A.; Shah, S. Q. N.; Bögge, H.; Schmidtmann, M. Molecular Growth from a Mo_{176} to a Mo_{248} Cluster. *Nature* **1999**, *397*, 48–50.
45. Müller, A.; Beckmann, E.; Bögge, H.; Schmidtmann, M.; Dress, A. Inorganic Chemistry Goes Protein Size: A Mo_{368} Nano-Hedgehog Initiating Nanochemistry by Symmetry Breaking. *Angew. Chem. Int. Ed.* **2002**, *41*, 1162–1167.
46. Falaise, C.; Khlifi, S.; Bauduin, P.; Schmid, P.; Shepard, W.; Ivanov, A. A.; Sokolov, M. N.; Shestopalov, M. A.; Abramov, P. A.; Cordier, S.; Marrot, J.; Haouas, M.; Cadot, E. "Host in Host" Supramolecular Core–Shell Type Systems Based on Giant Ring-Shaped Polyoxometalates. *Angew. Chem. Int. Ed.* **2021**, *60*, 14146–14153.
47. Moussawi, M. A.; Haouas, M.; Floquet, S.; Shepard, W. E.; Abramov, P. A.; Sokolov, M. N.; Fedin, V. P.; Cordier, S.; Ponchel, A.; Monflier, E.; Marrot, J.; Cadot, E. Nonconventional Three-Component Hierarchical Host–Guest Assembly Based on Mo-Blue Ring-Shaped Giant Anion, γ-Cyclodextrin, and Dawson-Type Polyoxometalate. *J. Am. Chem. Soc.* **2017**, *139*, 14376–14379.
48. Falaise, C.; Khlifi, S.; Bauduin, P.; Schmid, P.; Degrouard, J.; Leforestier, A.; Shepard, W.; Marrot, J.; Haouas, M.; Landy, D.; Mellot-Draznieks, C.; Cadot, E. Cooperative Self-Assembly Process Involving Giant Toroidal Polyoxometalate as a Membrane Building Block in Nanoscale Vesicles. *J. Am. Chem. Soc.* **2024**, *146*, 1501–1511.
49. Jiang, C.-C.; Wei, Y.-G.; Liu, Q.; Zhang, S.-W.; Shao, M.-C.; Tang, Y.-Q. Self-Assembly of a Novel Nanoscale Giant Cluster: $[Mo_{176}O_{496}(OH)_{32}(H_2O)_{80}]$. *Chem. Commun.* **1998**, *18*, 1937–1938.
50. Garrido Ribó, E.; Bell, N. L.; Xuan, W.; Luo, J.; Long, D.-L.; Liu, T.; Cronin, L. Synthesis, Assembly, and Sizing of Neutral, Lanthanide Substituted Molybdenum Blue Wheels $\{Mo_{90}Ln_{10}\}$. *J. Am. Chem. Soc.* **2020**, *142*, 17508–17514.
51. Li, X.-X.; Li, C.-H.; Hou, M.-J.; Zhu, B.; Chen, W.-C.; Sun, C.-Y.; Yuan, Y.; Guan, W.; Qin, C.; Shao, K.-Z.; Wang, X.-L.; Su, Z.-M. Ce-Mediated Molecular Tailoring on Gigantic Polyoxometalate $\{Mo_{132}\}$ into Half-Closed $\{Ce_{11}Mo_{96}\}$ for High Proton Conduction. *Nat. Commun.* **2023**, *14*, 5025.
52. Duros, V.; Grizou, J.; Xuan, W.; Hosni, Z.; Long, D.; Miras, H. N.; Cronin, L. Human Versus Robots in the Discovery and Crystallization of Gigantic Polyoxometalates. *Angew. Chem. Int. Ed.* **2017**, *56*, 10815–10820.
53. Xuan, W.; Pow, R.; Watfa, N.; Zheng, Q.; Surman, A. J.; Long, D.-L.; Cronin, L. Stereoselective Assembly of Gigantic Chiral Molybdenum Blue Wheels Using Lanthanide Ions and Amino Acids. *J. Am. Chem. Soc.* **2019**, *141*, 1242–1250.
54. Miras, H. N.; Mathis, C.; Xuan, W.; Long, D.-L.; Pow, R.; Cronin, L. Spontaneous Formation of Autocatalytic Sets with Self-Replicating Inorganic Metal Oxide Clusters. *Proc. Natl. Acad. Sci. U.S.A.* **2020**, *117*, 10699–10705.
55. She, S.; Xuan, W.; Bell, N. L.; Pow, R.; Ribo, E. G.; Sinclair, Z.; Long, D.-L.; Cronin, L. Peptide Sequence Mediated Self-Assembly of Molybdenum Blue Nanowheel Superstructures. *Chem. Sci.* **2021**, *12*, 2427–2432.
56. Liu, J.; Jiang, N.; Lin, J.; Mei, Z.; Dong, L.; Kuang, Y.; Liu, J.; Yao, S.; Li, S.; Lan, Y. Structural Evolution of Giant Polyoxometalate: From "Keplerate" to "Lantern" Type Mo_{132} for Improved Oxidation Catalysis. *Angew. Chem. Int. Ed.* **2023**, *62*, e202304728.
57. Wang, S.; Lin, X.; Wan, Y.; Yang, W.; Zhang, S.; Lu, C.; Zhuang, H. A Large, Bowl-Shaped $\{Mo_{51}V_9\}$ Polyoxometalate. *Angew. Chem. Int. Ed.* **2007**, *46*, 3490–3493.
58. Müller, A.; Krickemeyer, E.; Bögge, H.; Schmidtmann, M.; Peters, F. Organizational Forms of Matter: An Inorganic Super Fullerene and Keplerate Based on Molybdenum Oxide. *Angew. Chem. Int. Ed.* **1998**, *37*, 3359–3363.
59. Xuan, W.; Pow, R.; Long, D.; Cronin, L. Exploring the Molecular Growth of Two Gigantic Half-Closed Polyoxometalate Clusters $\{Mo_{180}\}$ and $\{Mo_{130}Ce_6\}$. *Angew. Chem. Int. Ed.* **2017**, *56*, 9727–9731.
60. Müller, A.; Shah, S. Q. N.; Bögge, H.; Schmidtmann, M.; Kögerler, P.; Hauptfleisch, B.; Leiding, S.; Wittler, K. Thirty Electrons "Trapped" in a Spherical Matrix: A Molybdenum Oxide-Based Nanostructured Keplerate Reduced by 36 Electrons. *Angew. Chem. Int. Ed.* **2000**, *39*, 1614–1616.
61. Gagné, O. C.; Hawthorne, F. C. Comprehensive Derivation of Bond-Valence Parameters for Ion Pairs Involving Oxygen. *Acta Crystallogr. Sect. B* **2015**, *71*, 562–578.
62. Xuan, W.; Surman, A. J.; Miras, H. N.; Long, D.-L.; Cronin, L. Controlling the Ring Curvature, Solution Assembly, and Reactivity of Gigantic Molybdenum Blue Wheels. *J. Am. Chem. Soc.* **2014**, *136*, 14114–14120.
63. Cronin, L.; Beugholt, C.; Krickemeyer, E.; Schmidtmann, M.; Bögge, H.; Kögerler, P.; Luong, T. K. K.; Müller, A. "Molecular Symmetry Breakers" Generating Metal-Oxide-Based Nanoobject Fragments as Synthons for Complex Structures: $[\{Mo_{128}Eu_4O_{388}H_{10}(H_2O)_{81}\}_2]_{20}$, a Giant-Cluster Dimer. *Angew. Chem. Int. Ed.* **2002**, *41*, 2805–2808.

Citation: *CCS Chem.* **2025**, Just Published. DOI: 10.31635/ccschem.025.202405353
Link to VoR: https://doi.org/10.31635/ccschem.025.202405353

64. Zhou, D.; Li, B.; Zhao, Q.; Tang, X.; Lan, T.; Su, H.; Yang, G.; Xuan, W. Solvent-Modulated Assembly of Peptide and Cerium Functionalized Gigantic $\{Mo_{120}Ce_6\}_2$ Dimers for High-Efficiency Photocatalytic Oxidation. *Inorg. Chem. Front.* **2024**, *11*, 2355–2364.
65. Miras, H. N.; Zang, H. Y.; Long, D.; Cronin, L. Direct Synthesis and Mass Spectroscopic Observation of the $\{M_{40}\}$ Polyoxothiometalate Wheel. *Eur. J. Inorg. Chem.* **2011**, *2011*, 5105–5111.
66. Robbins, P. J.; Surman, A. J.; Thiel, J.; Long, D.-L.; Cronin, L. Use of Ion-Mobility Mass Spectrometry (IMS-MS) to Map Polyoxometalate Keplerate Clusters and Their Supramolecular Assemblies. *Chem. Commun.* **2013**, *49*, 1909–1911.
67. Ian Buckley, R.; Clark, R. J. H. Structural and Electronic Properties of Some Polymolybdates Reducible to Molybdenum Blues. *Coord. Chem. Rev.* **1985**, *65*, 167–218.
68. Müller, A.; Serain, C. Soluble Molybdenum Blues"Des Pudels Kern." *Acc. Chem. Res.* **2000**, *33*, 2–10.
69. Chen, X.; Zhang, G.; Li, B.; Wu, L. An Integrated Giant Polyoxometalate Complex for Photothermally Enhanced Catalytic Oxidation. *Sci. Adv.* **2021**, *7*, eabf8413.
70. Xue, Y.-R.; Wang, Y.; Chen, G.; Sun, B.; Li, B.; Wu, L.; Wu, Y. A Hybrid HPV Capsid Protein L1 with Giant Mo-Containing Polyoxometalate Improves the Stability of Virus-like Particles and the Anti-Tumor Effect of $[Mo_{154}]$. *Biomater. Sci.* **2021**, *9*, 3875–3883.
71. Wang, Y.; Chen, G.; Liu, R.; Fang, X.; Li, F.; Wu, L.; Wu, Y. Synergistically Enhanced Photothermal Transition of a Polyoxometalate/Peptide Assembly Improved the Antibiofilm and Antibacterial Activities. *Soft Matter* **2022**, *18*, 2951–2958.

Citation: *CCS Chem.* **2025**, Just Published. DOI: 10.31635/ccschem.025.202405353
Link to VoR: https://doi.org/10.31635/ccschem.025.202405353